

# Source discrimination of mine water inrush using multiple methods: a case study from the Beiyangzhuang Mine, Northern China

Qiang Wu<sup>1</sup> · Wenping Mu<sup>1</sup> · Yuan Xing<sup>2</sup> · Cheng Qian<sup>3</sup> · Jianjun Shen<sup>1</sup> · Yang Wang<sup>1</sup> · Dekang Zhao<sup>1</sup>

Received: 13 December 2016 / Accepted: 31 October 2017 / Published online: 13 November 2017  
© Springer-Verlag GmbH Germany, part of Springer Nature 2017

**Abstract** The problem of distinguishing the source of water inrush in mines and tunnels has been addressed by studying the specific case of significant water inrush along the haulage roadway of the Beiyangzhuang Mine and applying three different methods to determine the source of the water inrush from a range of angles. The first of these methods was to determine the source by analyzing the dynamic response law of the groundwater in the water filling aquifers, including a Quaternary porous aquifer and a Cambrian–Ordovician karst aquifer. The second was to establish a linear equation for stratum burial depth and ground temperature to calculate water temperature. The source of water inrush is identified by comparing the calculated water temperature for the filling aquifer and the measured water temperature at the water inrush point. The third was to analyze the hydrochemical types of the water filling aquifers and water inrush point samples using a Piper diagram, followed by Fisher discriminant analysis to discriminate water inrush sources with eight hydrochemical components; the mixture ratio is roughly evaluated based on chloride mass balance. These three methods consistently showed that the primary source of water inrush is karst water. The hydrogeochemistry discrimination analysis further indicated that the mixing ratio of karst water to pore water was about

6.0, suggesting that this method is the powerful and more practical of the three methods tested. The results presented here provide significant guidance for the management of mine water inrush.

**Keywords** Source discrimination of water inrush · Water filling aquifers · Groundwater dynamic · Groundwater temperature · Hydrogeochemical characteristics · Fisher discriminant analysis · Mixing calculation

## Introduction

Water inrush in mines and tunnels can lead to serious disasters anywhere in the world, but particularly in parts of China due to the complicated hydrogeological conditions found in these areas and which are uncommon elsewhere in the world (Zhang 2005; Li et al. 2014; Yang et al. 2015; Ma et al. 2016; Sun et al. 2016; Wu et al. 2016; Zeng et al. 2016a, b). The highest recorded rates of water inrush have occurred at the Fangezhuang Coal Mine in Tangshan in 1984 (Meng et al. 2012), the Dongpang Coal Mine of Xingtai in 2003, the Luotuoshan Coal Mine of Wuhai in 2010, and the Yeshanguan Tunnel on the Yiwan Railway in 2007 (Zhou et al. 2015), with rates of 2053, 1270, 1167, and 1678 m<sup>3</sup>/min, respectively. Multiple water filling aquifers are often associated with tunnel and mine water inrush disasters (Wu and Wang 2006; Yin et al. 2015). Consequently, rapid and accurate discrimination of the source of the water inrush is very important and necessary, for both rescuing miners (construction workers) and resuming production (construction).

The groundwater level, groundwater temperature, and hydrochemical components are the important information sources for determining the characteristics of water filling aquifers. Based on these parameters, various identification

✉ Wenping Mu  
muwpcumtb@163.com

<sup>1</sup> National Engineering Research Center of Coal Mine Water Hazard Controlling, China University of Mining & Technology (Beijing), Beijing 100083, China

<sup>2</sup> Water Authority of Chaoyang District, Beijing 100026, China

<sup>3</sup> School of Water Resources and Environment, China University of Geosciences (Beijing), Beijing 100083, China

methods to identify water inrush sources have been proposed by international scholars. These methods can be divided into three categories: (1) groundwater head and groundwater temperature analysis methods (Sui et al. 2011; Chen et al. 2013; Lin et al. 2015); (2) hydrogeochemical analysis methods, based on the conventional component, including hydrogeochemical classification diagrams, multivariate statistical analyses, fuzzy evaluations, and neural networks (Sun 2013; Wang et al. 2016); (3) isotopes and trace elements analysis methods (Négrel et al. 2003; Yang and Huang 2007; Chen et al. 2010; Potot et al. 2012).

Hydrochemistry is widely used to identify water sources in hydrogeology. Examples of the use of hydrochemistry and isotopes in this context are the interaction relationship between deep groundwater and shallow groundwater (Petitta et al. 2011); the hydraulic connection between groundwater and surface water (Li et al. 2017); the recharge sources of groundwater (Kuroda et al. 2017); the seawater intrusion in the coastal aquifer (Najib et al. 2017); the flow path of groundwater (Wang et al. 2013), among others. The Piper diagram is a useful tool for identifying water recharge sources based on the chemical classification of groundwater. Further, chlorine-37 and oxygen-18 isotope ratio analysis is used to quantitatively evaluate the mixing ratio of groundwater from different aquifers based on mass conservation due to their maintenance of this ratio under most conditions (Subyani 2004; Mathurin et al. 2012; Liu and Amanaka 2012; Gu et al. 2017).

In recent years, many mathematical methods of source identification for mine water inrush have been proposed based on these conventional hydrochemistry components; these are fast, economical, and effective. Ma et al. (2014) establish a discriminant method of water inrush sources using the fuzzy evaluation, but its major flaw is that the maximum and minimum operations may lose large amounts of information on hydrogeochemical characteristics, leading to the problem of unclear classification (Cheng 1997). In order to overcome this problem, the unascertained clustering average method is proposed to identify water inrush sources (Zhang et al. 2014); however, the weakness of this method is that the judgment sets were designed subjectively. Another discriminant method of water inrush sources which does not require judgment sets which are subjectively designed is the extension identification (Zhang et al. 2009). In addition, the discriminant analysis methods based on the theory of multivariate statistical are applied to determine water inrush sources, such as the distance discriminant, the Bayes discriminant, among others (Chen et al. 2009b, 2010; Zhou et al. 2010). These methods obtain relatively satisfactory identification results. In order to further assure accuracy rate, a coupled identification model of water inrush sources is established based on gray relational and stepwise discriminant analysis (Xu et al. 2012). In addition, the artificial neural network and support vector machines are applied to

identify water inrush sources and other characteristics (Feng et al. 2002; Liu and Liu 2012), but both of these approaches require abundant training samples (Wu et al. 2017). Although such quantitative research studies have resulted in major progress in the single source discrimination of water inrush, they are characterized by two major limitations. The first is that they fail to identify multiple sources and evaluate their mixture ratio because of inherent defects in the methods themselves, and the second is that the quantitative calculation is emphasized and the analysis of hydrochemistry characteristics is ignored.

Considering all of the aforementioned problems and the comparison of the results of these different methods, in the study reported here we decide to apply three different discrimination methods to identify water sources, namely, the discrimination of groundwater dynamics, of groundwater temperature and of hydrogeochemistry parameters. The discrimination of groundwater dynamics is the most direct means to discriminate water inrush sources despite the complexity of hydrogeological conditions and it facilitates an analysis of the recharge conditions of the water filling aquifer. The discrimination of groundwater temperature is an indirect means to discriminate water inrush sources, and its merit is that it approximately provides the vertical location of the main source of water inrush when the mixture of multiple sources is not obvious. The hydrogeochemistry discrimination method not only discriminates multiple sources of water inrush, but also evaluates their mixture ratio. In our study, we focus on this latter method.

The hydrogeochemistry discrimination method consists of properly integrating the Piper diagram, Fisher discriminant analysis (FDA) and chloride mass balance. First, the Piper diagram is used to determine the chemical classification of the groundwater; second, FDA is used to discriminate the source of water inrush and analyze the mixture model (Chen et al. 2009a; Huang and Chen 2011); finally, the chloride ion analysis is used to roughly evaluate the individual contribution of each source. In our study we discriminate the source of water inrush using this method and subsequently verify its effectiveness by applying it to the Beiyangzhuang Coal Mine.

The Beiyangzhuang Coal Mine, about 220 km from Beijing, is located in Yuxian County, Hebei province, Northern China (Fig. 1). To guarantee the safety of mining in the No. 5 coal seam in the second mining area, the mine established a program of detecting and discharging groundwater in the filling aquifers using borehole No. 1 on June 4, 2014 and subsequently of detecting and discharging groundwater in the filling aquifers at borehole No. 2 on August 1, 2014. The average rate of mine drainage was found to be 300 m<sup>3</sup>/h. On September 27, a large amount of water was sprayed on the coal wall of the haulage roadway at a distance of 20 m around the No. 2 borehole with the elevation of the inrush point at about 430 m (Figs. 2, 3 and 4). The rate of water inrush

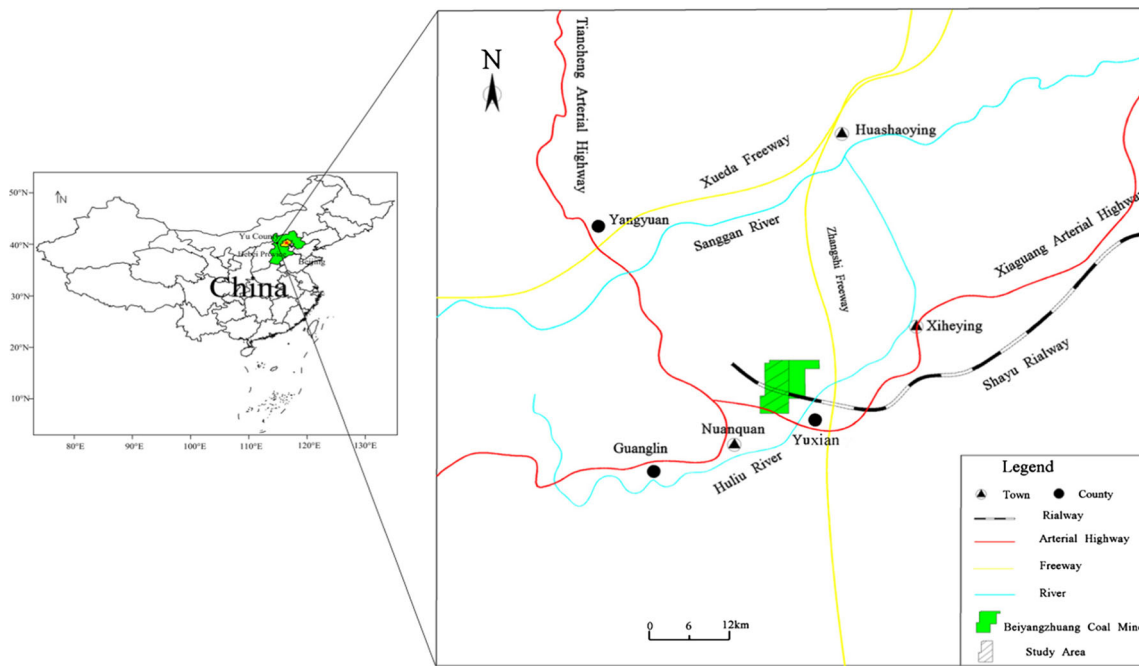
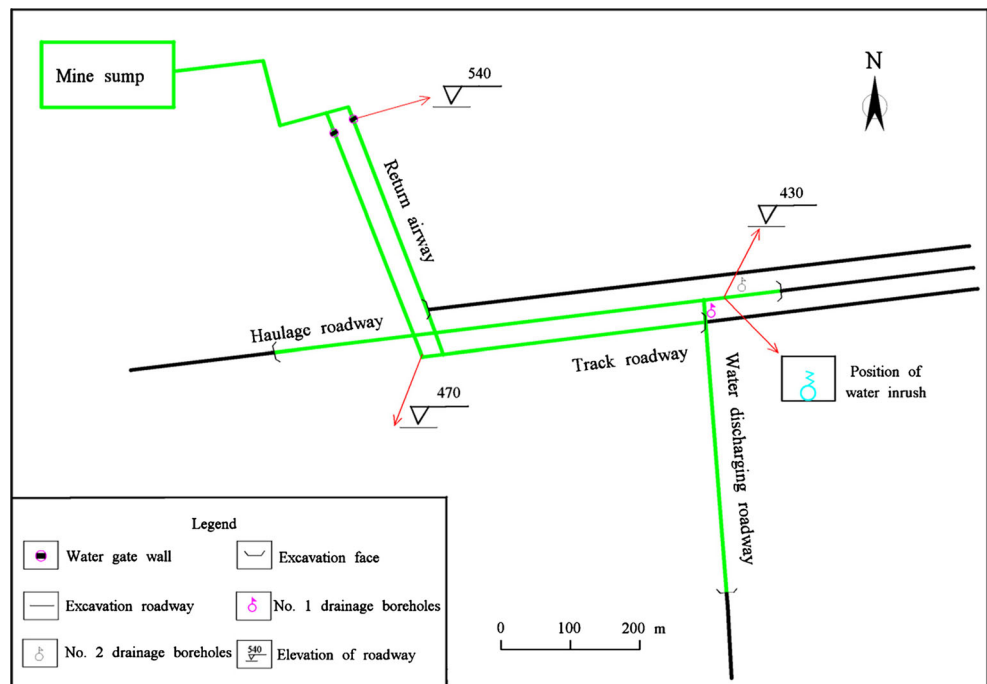


Fig. 1 Geographical location of the study area

increased from 550 to 2200 m<sup>3</sup>/h between September 27 and November 2. On November 3, underground drainage equipment and personnel were moved to the water gate wall where they began to drain water using the valves and pipes of the water gate wall in the roadway. The average rate of water inrush was 1800 m<sup>3</sup>/h between November 3, 2014 and July 7, 2015. The water pressure on the braced water gate walls was tested three times in early December 2014, early

April 2015, and late May 2015. The third test showed that the strength of the water gate walls was sufficient to resist the water pressure. The valves of the water gate wall were closed during this period. The water inrush pathway was stopped by applying ground grouting technology between July 7, 2015 and August 10, 2015 (Wang et al. 2011). The water gate wall pipe began drainage on August 18, 2015, and the average rate of mine drainage quickly dropped to 50 m<sup>3</sup>/h.

Fig. 2 Planimetric position of the water inrush point and roadway engineering



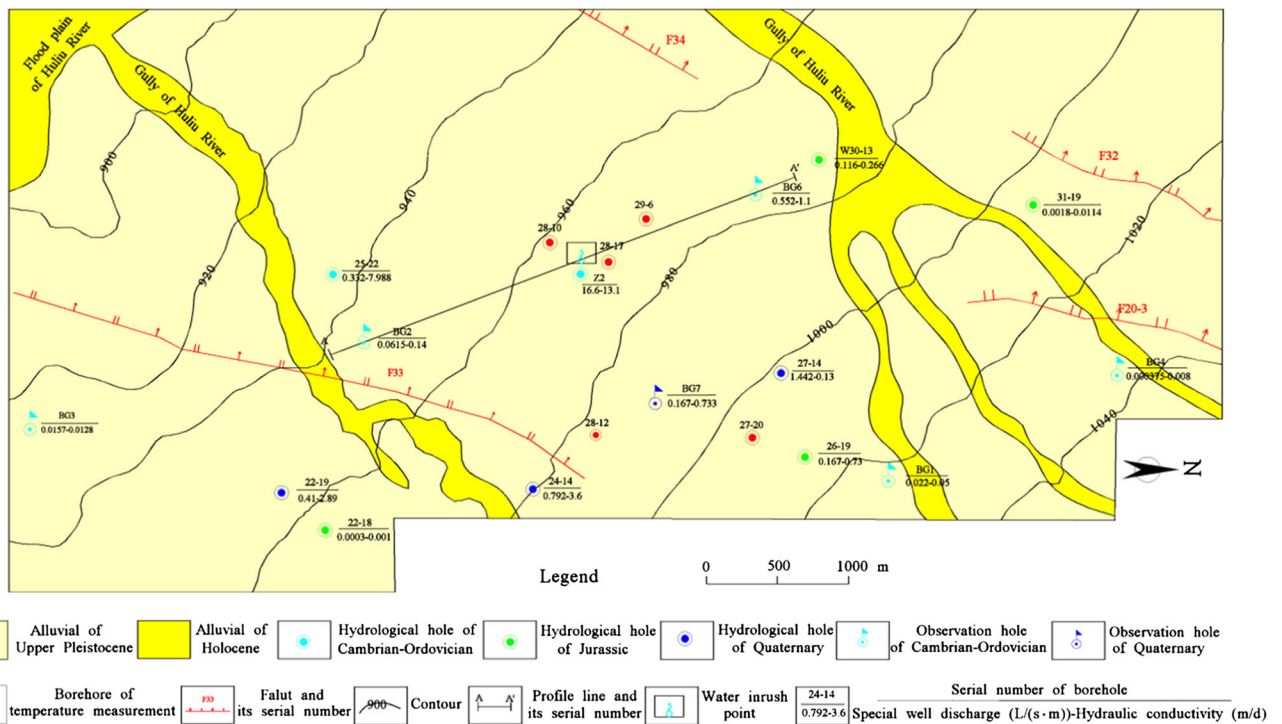


Fig. 3 Geological map of the study area and the location of observation holes

### Geological and hydrogeological conditions

The study area is located in the eastern part of the Beiyangzhuang Mine (Fig. 1), which is located in a semi-arid region with a long-term average precipitation of 400 mm/year, concentrated between June and September. The Huli River is a perennial river, located to the south of study area. Two gullies, which channel seasonal rivers, have developed on the surface, forming the first tributaries. The

geomorphology is dominated by the Huli River alluvial plain. The topography is high in the northwest and low in the southeast with a surface elevation varying from 900 to 1040 m a.s.l. (Fig. 3).

The study area is a synclinal structure with a northeast-oriented axial trend and an average inclination angle on the limbs of about 10° (Fig. 4). The main faults in the area are denoted as F33, F20–3, F32, and F34 (Fig. 3). According to the geological condition exposure situation of the roadway,

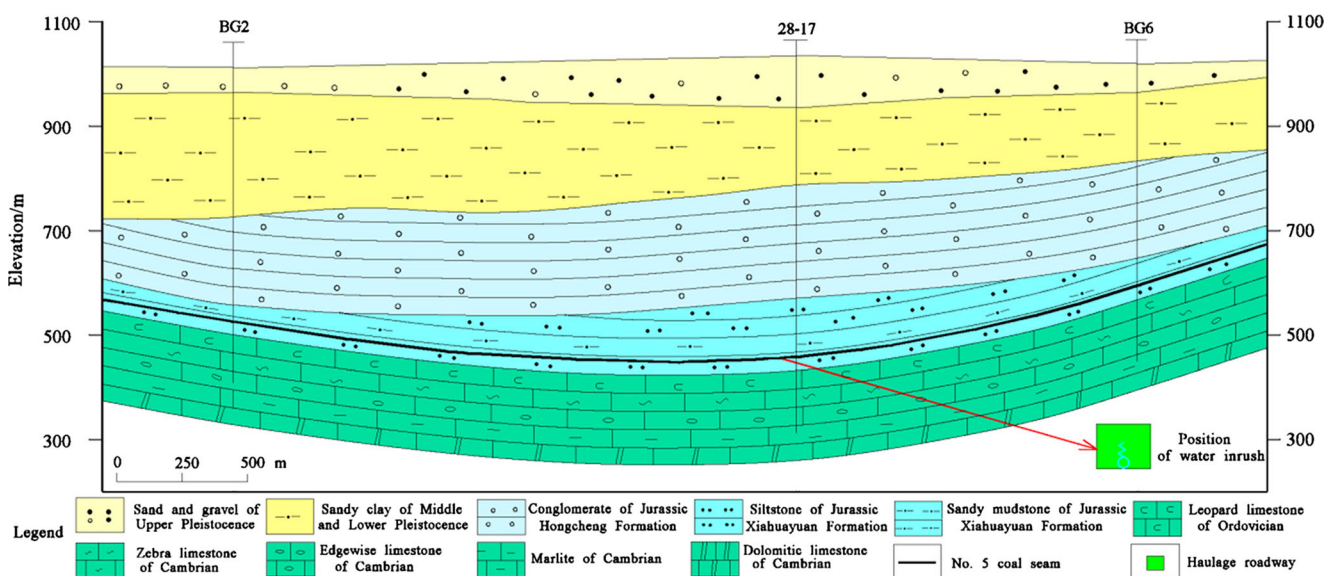


Fig. 4 A–A' profile in Fig. 3

well-developed faults are present at a fault distance of less than 7 m. Cambrian–Ordovician carbonate rocks, Jurassic clastic rocks, and Quaternary alluvial deposits are the main strata in the region. Edgewise limestone and thin-layer limestone are located in the upper part of the Cambrian; dolomitic limestone and oolitic limestone are located in the middle (Fig. 5); mudstone and marlstone are located in the lower part. The Ordovician lithology is dominated by leopard limestone (Fig. 5). The Jurassic clastic sediments are characterized by a dual structure where the upper part is conglomerate and the lower part is siltstone. The Quaternary alluvial deposits are also characterized by a dual structure where the lower part is silty clay and the upper part is gravel. The No. 5 coal seam layer can be exploited in the lower part of the Jurassic (Fig. 4).

The main water filling aquifers include Cambrian and Ordovician limestone karst water, Jurassic conglomerate fissure water and Quaternary sand and gravel pore water. The main aquicludes include Jurassic siltstones and mudstones and a Quaternary silty clay layer. The spatial structure of the aquifers and the aquicludes shows that they overlap in the vertical direction and are distributed as layers in the plane (Fig. 4).

The Cambrian limestone karst aquifers are more than 100 m thick and the thickness of the Ordovician karst aquifer is less than 50 m. The Cambrian and Ordovician karst aquifers have similar hydraulic connections, which form a thick karst fissure water-bearing rock mass. The hydraulic conductivity of the karst aquifer ranges from 0.008 to 13.1 m/day, with an average of 3.2 m/day, and the special well discharge ranges from 0.0004 to 16.6 L/(m·s) with an average of 2.51 L/(m·s). The thickness of the Jurassic conglomerate fissure aquifer ranges from 150 to 200 m. The hydraulic conductivity of the Jurassic aquifer ranges from 0.001 to 0.73 m/day, with an average of 0.25 m/day, and the special well discharge ranges from 0.0003 to 0.167 L/(m·s) with an average of 0.07 L/(m·s).

The thickness of the Quaternary sand and gravel pore aquifer ranges from 150 to 200 m. The hydraulic conductivity of the Quaternary sand and gravel aquifer ranges from 0.13 to 3.6 m/day, with an average of 1.83 m/day, and the special well discharge ranges from 0.17 to 1.44 L/(m·s), with an average of 0.70 L/(m·s) (Fig. 3). It follows that there is a very obvious difference in the permeability and water yield property of the karst aquifer in different regions because of the significant heterogeneity.

## Theory and methods

### Sample collection

The observation data of groundwater level is obtained from six observation holes (Figs. 3, 6). The series ground temperature data of borehole 27-20 and the scatter ground temperature data of another four boreholes are also collected (Fig. 7; Table 1), along with 33 groundwater samples: eight from the Quaternary pore aquifer, 11 from the Jurassic fissure aquifer, and 14 from the Cambrian–Ordovician karst aquifer. Additionally, three water samples are taken from the water inrush point (Table 2). The samples are tested for eight parameters, including major cations ( $K^+$ ,  $Na^+$ ,  $Ca^{2+}$ ,  $Mg^{2+}$ ), major anions ( $HCO_3^-$ ,  $CO_3^{2-}$ ,  $SO_4^{2-}$ ,  $Cl^-$ ), pH, and total dissolved solids (TDS).

### Principle of the groundwater dynamic response

According to the principle of water balance and groundwater system theory, when a groundwater system receives input information, after conversion by the geological body, it must produce output information. The degree of the response between inputs and outputs is controlled by the hydrogeological

**Fig. 5** Typical core from borehole Z2



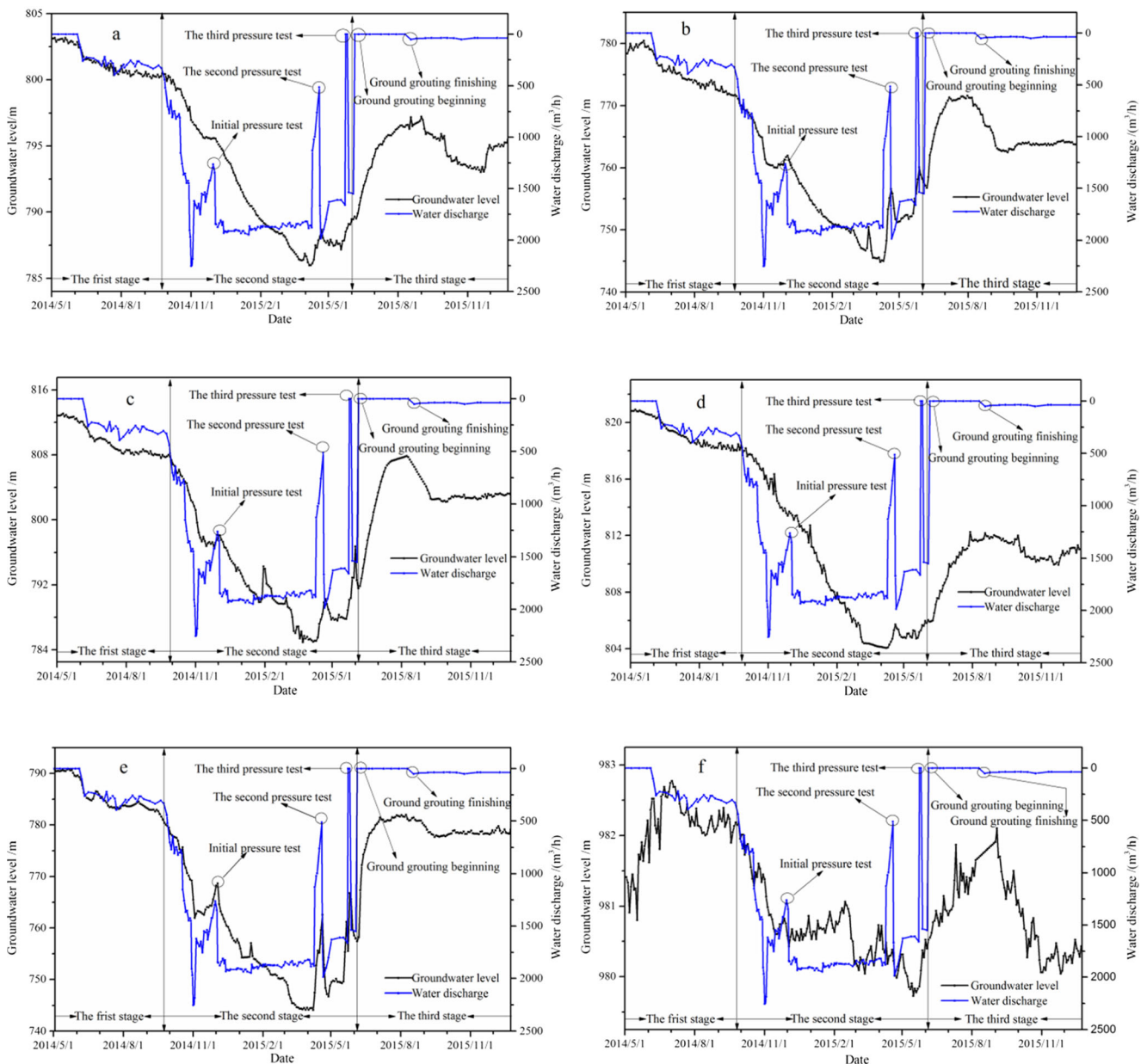


**Fig. 6** Dynamic change observed in the groundwater observation borehole and mine drainage. **a** Groundwater observation borehole G1, **b** groundwater observation borehole G2, **c** groundwater observation

borehole G3, **d** groundwater observation borehole G4, **e** groundwater observation borehole G6, **f** groundwater observation borehole G7

conditions. The relationship of inputs (e.g., the rate of water inrush) and outputs (e.g., groundwater level) is described by Eq. 1 (Xu and Shao 1988), which indicates that the mine water inrush must decrease the groundwater level in the aquifer.

$$s(x_i, x_j, t) = \int_0^t Q(x_i, \tau) \beta(x_i, x_j, t - \tau) d\tau, 0 \leq \tau \leq t \quad (1)$$

where  $x_i$  and  $x_j$  are the coordinates of  $i$  and  $j$ , respectively;  $Q(x_i, \tau)$  is the rate of water inrush at time  $\tau$  in  $i$ , ( $\text{m}^3/\text{day}$ );  $s(x_i, x_j, t)$  is the groundwater drawdown of  $j$  due to water inrush at rate  $Q(x_i, t)$  in  $i$ , (m);  $\beta(x_i, x_j, t - \tau)$  is the groundwater

drawdown of  $i$  due to pumping groundwater with specific rate of flow during the time  $t - \tau$ , (m).

### Hydrochemical piper diagram and FDA

Under the condition of no mixing or no obvious mixing effects, the hydrogeochemical characteristics of different aquifers may exhibit some differences, while there is a similarity in the hydrogeochemical characteristics of the same aquifer. This is the fundamental reason for identifying the source of water

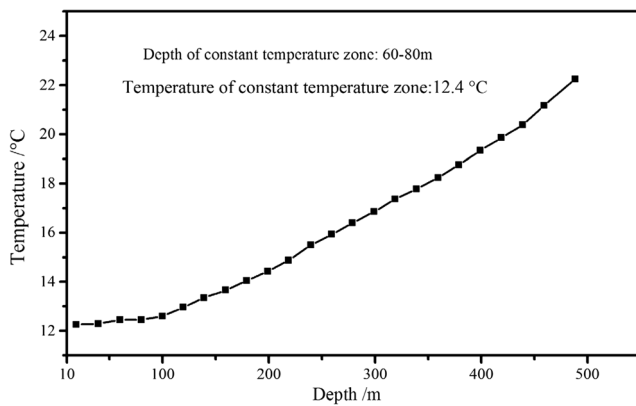


**Fig. 7** Temperature–depth curve for borehole 27-20

inrush based on hydrochemical composition. The Piper diagram and FDA are used to identify sources of water inrush based on hydrochemical compositions; in our study we used the AqQa version 1.1 water analysis software program (RockWare Inc., Golden, CO) and SPSS version 19 (IBM Corp., Armonk, NY), respectively, to study these parameters

Based on the hydrogeochemical analysis data, Piper diagrams have been widely used to classify the hydrochemical types of groundwater, analyze hydraulic connections in different aquifers, and gain an initial understanding of the chemical interaction between groundwater and minerals of surrounding rock hydrogeology according to the plotted position of water samples from different aquifers (Gültekin et al. 2013; Chemseddine et al. 2015; Li et al. 2015; Redwan and Abdel Moneim 2015; Qian et al. 2016).

FDA is one of many discriminant analysis methods, and it has been widely used for identification and classification in many fields of natural sciences based on observation data, such as face recognition (Liu et al. 2003), fault diagnosis (Chiang et al. 2004), disease diagnosis (Guo and Nandi 2006), risk identification of geologic hazard (Zhou et al. 2011), among others. FDA extracts features of raw data by dimensionality reduction. Its essence is to construct a discriminant function by maximizing the ratio between between-groups dispersion and within-groups dispersion using training samples (Chen et al. 2016). The discriminant function is used to calculate the

function value of the training samples and the unknown sample. Thereafter, the category of the unknown samples is determined according to the discrimination criterion of the minimum distance between the center of the training samples in each category and the unknown sample in the new coordinate system where the discriminant functions are used to represent the coordinate axis. For example, consider three categories  $G_I$  ( $I = 1, 2, 3$ ) where the sample number of each category is  $n_I$  ( $I = 1, 2, 3$ ).  $x_p$  ( $p = 1, \dots, 8$ ) is the indicator of each sample.

The discriminant function is defined as:

$$y = \sum_{p=1}^8 c_p x_p = c^T x \tag{2}$$

where  $c = (c_1, \dots, c_p)^T$  and  $x = (x_1, \dots, x_p)^T$ . and the deviation ratio is:

$$\lambda = \frac{\sum_{i=1}^3 n_i \left( \bar{y}^{(i)} - \bar{y} \right)^2}{\sum_{i=1}^3 (n_i - 1) \sigma_i^2} \tag{3}$$

where  $\bar{y}^i = c^T \bar{x}^i$ ,  $\sigma_i^2 = c^T \sum^i c$ ,  $\bar{y} = c^T \bar{x}$ .  $\bar{y}^i$  is the sample mean of the  $G_i$ ,  $\sigma_i^2$  is the sample variance of  $G_i$ ,  $\bar{y}$  is the total mean vector,  $\bar{x}^i$  is the mean matrix and  $\sum^{(i)}$  is the covariance matrix.

Equation 3 is converted into Eq. 4:

$$\lambda = \frac{c^T B c}{c^T E c} \tag{4}$$

where  $B = \sum_{i=1}^3 n_i (\bar{x}^i - \bar{x})(\bar{x}^i - \bar{x})^T$  and  $E = \sum_{i=1}^3 \sum_{j=1}^{n_i} (\bar{x}_j^i - \bar{x}_i)(\bar{x}_j^i - \bar{x}_i)^T$ .  $B$  and  $E$  are the between-groups dispersion matrix and the within-groups dispersion matrix, respectively.

The necessary condition for  $\max \lambda$  is  $\frac{\partial \lambda}{\partial c} = 0$ . Therefore, Eq. 4 is converted into Eq. 5:

$$Bc = \lambda Ec \quad (\lambda = 1, 2) \tag{5}$$

where  $\lambda$  and  $c$  are the characteristic root and the corresponding eigenvector of the matrix  $B^{-1}E$ , respectively;

**Table 1** The results of geothermal gradient in the study area

Boreholes	Ground surface elevation (m a.s.l.)	Depth of measure point A (m)	Temperature of measure point A (°C)	Depth of measure point B (m)	Temperature of measure point B (°C)	Average geothermal gradient (°C/100 m)
29-6	978	549.4	22.0	591.8	23.1	2.08
28-17	985	528.8	24.4	601.2	25.5	2.59
26-14	1003	428	23.2	500	25.0	3.05
28-12	944	512.5	24.3	564.1	25.5	2.73

**Table 2** Hydrochemical compositions and discriminant results of water filling aquifer and water inrush point

Groundwater type and classification letter	Water samples	Hydrochemical composition (mg/L)								Discriminant results
		pH	TDS	HCO <sub>3</sub> <sup>-</sup>	SO <sub>4</sub> <sup>2-</sup>	Cl <sup>-</sup>	Na <sup>+</sup> +K <sup>+</sup>	Ca <sup>2+</sup>	Mg <sup>2+</sup>	
Pore water of Quaternary sand and gravel (A)	P1	7.7	454	319.1	46.9	30.1	95.87	30.5	18.9	A
	P2	7.6	523	342.3	91.4	35.8	115	36.3	24.1	
	P3	7.7	645	389.8	116.5	48.6	158.9	31.9	32.5	
	P4	7.6	501.7	408	51.3	27.6	152	14.2	21.2	
	P5	8.8	351.3	282.2	6.6	27.8	128	10.3	4.2	
	P6	7.8	312	249.5	36.2	25.2	36.3	46.7	21.5	
	P7	7.8	398.4	368.4	50.5	13.1	90.5	39.0	19.8	
	P8	7.7	564.8	580.5	72.6	2.9	192.5	27.7	17.3	
Fissure water of Jurassic conglomerate (B)	F1	8.2	1496	1232	52.5	120.8	543.2	13.6	6.2	B
	F2	8.2	1367	792.2	42.1	144.2	404.7	10.2	0.5	
	F3	8.0	1454	855	31.6	124.7	845.6	8.5	1.0	
	F4	8.5	971.9	585.6	51.3	180.8	365	6.0	4.6	
	F5	8.5	980	611.9	66.7	151.8	389	7.0	1.2	
	F6	8.2	868	693.5	5.4	142.2	343.1	8.2	1.7	
	F7	7.8	555.5	383.2	75.94	68.12	196.7	14.92	3.18	
	F8	8.6	973.6	726.6	114.4	65.5	373	7.47	4.5	
	F9	8.5	1355	848.2	171.2	98.8	517.5	9.2	2.8	
	F10	8.3	796	574.6	2.26	168.6	316.5	9.6	2.4	
	F11	8.2	647.5	392.5	30.25	30.25	246.5	9.8	4.5	
Karst water of Cambrian–Ordovician limestone (C)	K1	8.4	637.7	288.5	179.6	80.34	129.6	34.1	52.5	C
	K2	8.4	585.8	145.9	183.9	93.4	162.3	33.0	20.2	
	K3	7.2	591.1	319	89.3	27.7	72.2	41.8	34.3	
	K4	7.7	830.2	398.7	61.2	149.6	164.4	57.1	26.9	
	K5	7.1	607.5	184.2	131.3	117.4	83.5	58.4	31.8	
	K6	7.4	425.7	276	106.9	33.1	41.1	71.4	32.3	
	K7	8.1	566.1	272.9	121.9	82.7	163.2	38.8	7.6	
	K8	7.7	1514	704.2	194.9	200.4	409.3	15.49	33.9	
	K9	7.0	720	355.8	119.9	50.4	118	48.5	25.7	
	K10	7.7	920.7	415.6	115.1	119.4	206	39.5	21.0	
	K11	7.7	892.4	346.2	121.2	160.6	200	38.8	23.6	
	K12	7.9	903.2	340.5	135.5	157.9	190	55.6	19.8	
	K13	7.4	825	349.8	119.6	126.9	148	51.3	27.3	
	K14	8.1	740	284.3	147.4	163.1	159.6	71.34	22.5	
Samples of water inrush point	I1	6.9	956.7	501	167.9	25.1	151.7	36.0	50.3	C
	I2	6.8	783	362.5	168.2	50.5	160.4	35.5	27.6	
	I4	7.5	605.5	297.3	168.9	75.6	121.3	55.1	31.3	

The serial number of water samples starting with P, F, and K successively indicate pore water, fissure water, and karst water. I1, I2, and I4 samples were collected on 29 and 29 September 2014 and on 21 May 2015, respectively

TDS, Total dissolved solids

the non-zero eigenvalues are  $\lambda_1$  and  $\lambda_2$ , respectively; the corresponding eigenvectors are  $c_1^T$  and  $c_2^T$ , respectively. From this we can determine the discriminant function as:

$$y = c_l^T x \quad (l = 1, 2)$$

(6)

The distance between the location of the unknown sample and the center of the training samples in the coordinate system is defined as:

$$D_i = \sqrt{\left(y_1 - \bar{y}_1^i\right)^2 + \left(y_2 - \bar{y}_2^i\right)^2} \quad (7)$$



where  $y_1$  is the value of the discriminant function 1 of the unknown sample, and  $y_2$  is the value of the discriminant function 2 of the unknown sample.  $\bar{y}_1^i$  is the average value of the discriminant function 1 of training samples in the  $i$  category, and  $\bar{y}_2^i$  is the average value of the discriminant function 2 of the unknown sample in the  $i$  category.

The identification ability of the discriminant functions is defined as:

$$P_l = \frac{\lambda_l}{\sum_{l=1}^2 \lambda_l} \quad (l = 1, 2) \quad (8)$$

## Results and discussion

### Discrimination of groundwater dynamics

The plane position of the Cambrian–Ordovician karst water observation holes and the Quaternary pore water observation holes is shown in Fig. 3. According to the dynamic characteristics of the groundwater as applied to an engineering background, the dynamic curve can be divided into three stages: the first phase (May 1, 2014–September 27, 2014) was a stage of water detection and drainage; the second stage (September 27, 2014–June 7, 2015) was the stage of water inrush; the third stage (June 7, 2015–December 24, 2015) was the stage of groundwater level recovery. The time dividing point between the first and second stages was the time of water inrush onset in the mine roadway. The time dividing point between the second and the third stage coincided to the time of grouting initiation on the ground.

During the first stage, the average rate of water drainage was approximately 300 m<sup>3</sup>/h, while the average rate of water inrush was approximately 1800 m<sup>3</sup>/h in the second stage. The average rate of the water flow was approximately 50 m<sup>3</sup>/h in the third stage. The hydraulic head at the karst water observation holes BG1, BG2, BG3, BG4, and BG6 decreased by 3, 8, 5, 2, and 8 m, respectively, during the first stage. The maximum drawdown at karst water observation holes BG1, BG2, BG3, BG4, and BG6 decreased by 14.5, 30, 22, 13.8, and 42 m, respectively, in the second stage. The hydraulic head at karst water observation holes BG1, BG2, BG3, BG4, and BG6 then recovered 7.5, 15, 16, 6, and 22 m, respectively, in the third stage (Fig. 6a–e).

There is a strong negative correlation between the dynamics of karst water and the change in water inrush rates during the second stage. The dynamic curve of karst water is gentler than that of the water inrush rates, which shows that the groundwater system has a regulation function. Moreover, the slope of the karst water dynamic curve at the beginning of the

second stage is much higher than that at the first stage because of mine water inrush (Fig. 6a–e). The slope of the karst water dynamic curve changes from high to low in the second stage and finally reaches 0, which indicates that the status of the karst groundwater near the water inrush point gradually develops from an unsteady flow to a steady flow with the expansion of the groundwater depression cone.

When the rate of water inrush decreases due to gradual closing of the valves of the water gate wall in the process of testing water pressure, the hydraulic head of the karst water observation hole will increase immediately. When the rate of water inrush increases due to gradual opening of the valves of the water gate in the process of testing water pressure, the hydraulic head of the karst water will decrease immediately. The dynamic response of karst water observation hole BG6 was the most obvious of all the observation holes; over the course of the water pressure tests, the hydraulic head at observation hole BG6 increased by 5, 15 and 18 m, respectively, and then decreased by 5, 16 and 10 m, respectively (Fig. 6a–e).

The dynamics of the karst water lags behind the dynamics of water inrush rate in three pressure tests. The lag times of the dynamics for observation holes BG1, BG2, BG3, and BG4 are much longer than that of BG6; so are the response amplitudes (Fig. 6a–e), which are related to the permeability of the aquifer and the distance between the water inrush point and the observation hole (Fig. 3).

The amplitude of the hydraulic head at pore water observation hole BG7 was about 2 m at the whole drainage stage. The head at hole BG7 showed periodic overall fluctuations, with a local small elevation in amplitude from May to July 2014, a decline from August to November, a slight increase from December 2014 to February 2015, and then a slight decline from March to May 2015. There are a number of factors that can account for this pattern. First, as much as 70% of the annual precipitation in the region occurs between May and August, and this precipitation is the main source of pore water recharge during the year. Second, snowmelt is the other source of pore water from the previous December to the following February. Third, pore water groundwater is exploited for agricultural irrigation from April to May. Regardless of water inrush, the dynamics of hole BG7 presents fluctuations in the second stage (Fig. 6f). These results suggest that pore water has little relation with water inrush.

The slope of the water head recovery curve represents the renewable capacity of the karst aquifer. As shown in Fig. 6a–e, the recovery is strongest for hole BG6, with the next strongest being the BG2 and BG3 holes, and the weakest being holes BG1 and BG4. Under these conditions, the average rate of water inrush is 1800 m<sup>3</sup>/h, which is equal to the water supply of a drinking water source area for a small city, and the time of water inrush is 7 months. The hydraulic head of observation holes BG1, BG2, BG3, BG4, and BG6 finally decreased by 3,

6, 16, 12, and 22 m, respectively. After the water level recovery, the hydraulic head of observation holes BG1, BG2, BG3, BG4, and BG6 was only lower by 3, 6, 6, 6, and 4 m, respectively, than that observed before the water inrush. These observations show adequate karst development and sufficient recharge conditions of groundwater near the water inrush point and also show that the static reserves of groundwater resources are consumed in the process of water inrush.

Unfortunately, the groundwater level in the Jurassic fissure aquifer is not monitored in the water inrush process, so we could not determine whether the water inrush involves fissure water. Because the water yield property of the fissure aquifer is weak (Fig. 3), it is difficult to provide enough water. The above analysis shows that primary source of water inrush is karst water, that the recharge conditions of karst water is good, and that the static-storage of karst water resources near the water inrush point is relatively abundant based on groundwater dynamics. The water recovery curve during the third stage further shows that the recognition results are correct. These analysis also shows that it is a effective means with respect to the ground grouting technology for stopping the path for water inrush, although the single dewatering step is impractical.

### Discrimination of groundwater temperature

According to the measurement curve of the steady state ground temperature in borehole 27-20 (Fig. 3), the depth of the constant temperature layer is 60–80 m and the constant temperature is 12.4 °C in the mine (Fig. 7). Based on the linear relationship between the ground temperature and the burial depth of the stratum (Abdula 2017), the ground temperature gradient can then be calculated using the simple temperature measurement data of four boreholes near the water inrush point (Table 1). A linear regression equation between the ground temperature and depth is obtained by taking the mean of the geothermal gradient at each measuring point:

$$T = 12.4 + 2.6 \frac{H-80}{100} \quad (9)$$

where  $T$  is the ground temperature in degrees celsius and  $H$  is the depth of the stratum in meters.

According to Eq. 9, the temperatures of the Quaternary pore water and Jurassic fissure water are 14.8 °C and 21.3 °C, respectively. Moreover, the groundwater temperatures in the roof and floor of Cambrian–Ordovician aquifer are 25.7 °C and 31.1 °C, respectively, with an average of 28.8 °C. The measured water temperature of the water inrush point is 31 °C, which is very close to the water temperature of the karst aquifer. The thermal insulation effect of Jurassic sand

and mudstone may cause the geothermal gradient to be slightly higher than the calculated average value (Fig. 4).

The above analysis illustrates that the main source of water inrush is karst water coming from the middle and lower part of the Cambrian–Ordovician karst aquifer. If the grouting is selected to manage water inrush, the results show that the grouting between the upper part of the karst aquifer and the water inrush point can cut off the water inrush source. When the distance between a water filling aquifer and another water filling aquifer is short, the discrimination of groundwater temperature is inapplicable.

### Hydrogeochemistry discrimination

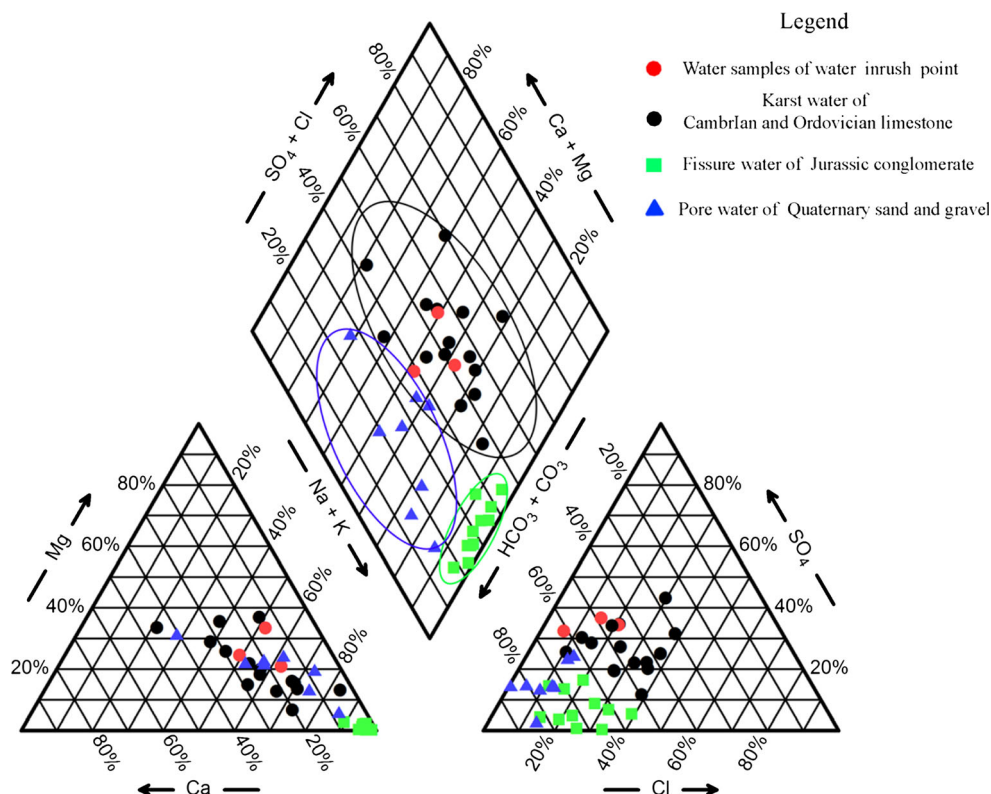
#### *Hydrochemical characteristics*

Hydrogeochemical characteristics of water filling aquifers and water samples from water inrush points are analyzed using a Piper diagram (Table 2). The hydrochemical types of Ordovician–Cambrian karst water are mainly  $\text{HCO}_3^- \cdot \text{Cl}^- \cdot \text{Na}^+$  and  $\text{HCO}_3^- \cdot \text{SO}_4^{2-} \cdot \text{Na}^+ \cdot \text{Mg}^{2+} (\text{Ca}^{2+})$  (Fig. 8). The average content of TDS is about 0.7 g/L (Table 2). This analysis shows that karst water circulation conditions are relatively good. The content of bicarbonate, magnesium, and calcium ions is high due to the dissolution of calcite and dolomite in karst water. In addition, ion exchange between calcium and sodium ions can result in high sodium content. The sulfate ion content in karst water is obviously higher than that found in the Quaternary pore water or the Jurassic fissure water (Table 2), which is interpreted to be the result of the dissolution of the gypsum inter-layers in the Ordovician and Cambrian limestone.

The hydrochemical types of the Jurassic fissure water are  $\text{HCO}_3^- \cdot \text{Na}^+$  and  $\text{HCO}_3^- \cdot \text{Cl}^- \cdot \text{Na}^+$  (Fig. 8), which are relatively simple. The average content of TDS is about 1.1 g/L (Table 2). Due to the low permeability of the aquifer and the dissolution of silicate and sodium chloride in the fissure water, the main cation is  $\text{Na}^+$  and the main anions are  $\text{HCO}_3^-$  and  $\text{Cl}^-$ . As the bicarbonate ion content is much higher than in the other two types of groundwater, the pH is also higher. Due to the close hydraulic connection and frequent conversion relationship between the Quaternary pore water and atmospheric precipitation, its hydrochemistry type is  $\text{HCO}_3^- \cdot \text{Ca}^{2+} \cdot \text{Mg}^{2+}$  (Fig. 8), and the average content of TDS is about 0.4 g/L (Table 2).

The hydrochemical types of the water samples at the water inrush point are  $\text{HCO}_3^- \cdot \text{SO}_4^{2-} \cdot \text{Na}^+ \cdot \text{Mg}^{2+} (\text{Ca}^{2+})$  (Fig. 8), which exactly match those of karst water and are somewhat similar to those of pore water, although they are clearly different from the hydrochemical types of fissure water. This profile indicates that the main source is karst water and that a small part of the source may be pore water. As shown in Fig. 8, the hydraulic

**Fig. 8** Piper diagram of groundwater samples



connection is not close in the different water filling aquifers although there are some faults in the mine (Fig. 3). However, the fault activation which is induced by mining activities may lead to a water inrush involving pore water.

*Identification results of FDA*

In order to further discriminate the water source, we select eight hydrochemical components, namely, pH ( $x_1$ ), TDS ( $x_2$ ),  $\text{HCO}_3^-$  ( $x_3$ ),  $\text{SO}_4^{2-}$  ( $x_4$ ),  $\text{Cl}^-$  ( $x_5$ ),  $\text{Na}^+ + \text{K}^+$  ( $x_6$ ),  $\text{Ca}^{2+}$  ( $x_7$ ), and  $\text{Mg}^{2+}$  ( $x_8$ ), as water inrush identification indices according to the hydrogeochemical analysis described in preceding sections. For this analysis, the water samples of water filling aquifers are divided into three categories: A, Quaternary pore water; B, Jurassic fissure water; C, Cambrian–Ordovician karst water. In addition, water samples from the water inrush point are considered to be the uncertain category for the moment (Table 2).

The discriminant function is obtained using SPSS software, as shown in Eqs. 10 and 11. The significance level of the observations for discriminant function 1 (DF1) and discriminant function 2 (DF2) is  $1.6 \times 10^{-9}$  and  $6.0 \times 10^{-3}$  in the statistical test, respectively. Therefore, the significance level of the observations for the discriminant functions are much less than the given significance level, 0.05—which indicates that two

discriminant functions are valid. The value of  $P$  for DF1 and DF2 is 0.86 and 0.14, respectively, which indicates that the identification ability of DF1 and DF2 is 86 and 14%, respectively. These values suggest that DF1 plays a main role in identifying water inrush sources (Fig. 9). The standardized discriminant coefficient of pH ( $x_1$ ), TDS ( $x_2$ ),  $\text{HCO}_3^-$  ( $x_3$ ),  $\text{SO}_4^{2-}$  ( $x_4$ ),  $\text{Cl}^-$  ( $x_5$ ),  $\text{Na}^+ + \text{K}^+$  ( $x_6$ ),  $\text{Ca}^{2+}$  ( $x_7$ ), and  $\text{Mg}^{2+}$  ( $x_8$ ) in DF1 is  $-0.002$ , 1.41,  $-1.12$ ,  $-0.30$ ,  $-0.10$ ,  $-0.44$ , 0.63, and 0.34, respectively, which shows that TDS ( $x_2$ ),

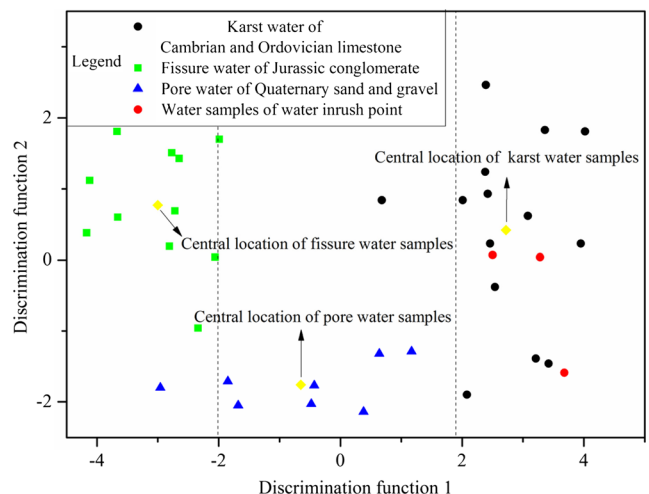


**Fig. 9** Distribution of water filling aquifers and water inrush point samples using Fisher discriminant analysis

HCO<sub>3</sub><sup>-</sup> (x<sub>3</sub>), and Cl<sup>-</sup> (x<sub>5</sub>) contribute greatly to the ability to identify water inrush sources.

$$y_1 = -0.0056x_1 + 0.0054x_2 - 0.0066x_3 + 0.0087x_4 - 0.0023x_5 - 0.0037x_6 + 0.0531x_7 + 0.0460x_8 - 3.21 \tag{10}$$

$$y_2 = -0.1159x_1 + 0.0016x_2 - 0.001x_3 + 0.0119x_4 - 0.0119x_5 + 0.001x_6 + 0.0128x_7 - 0.0652x_8 - 1.445 \tag{11}$$

The plane position of the unknown samples and the training samples is determined by DF1 and DF2. The pore water samples, the fissure water samples, karst water samples, and water inrush point samples are seen to be distributed on the left side of Fig. 9, the middle of the Fig. 9, the right side of Fig. 9, and the right side of Fig. 9, respectively. Also shown in Fig. 9, the water samples are differentiated in a new coordinate system composed of DF1 and DF2.

The distance between the location of the water inrush point samples and the central location of the karst water samples is shorter than the location of the water inrush point samples and the central location of the water samples from the other categories. The distance between the location of the water inrush point samples and the central location of the fissure samples is much longer than the location of water inrush point samples and the central location of the pore water samples (Fig. 9; Table 3). The average distance of the location of water inrush point samples to the central location of pore water samples and to the location of fissure water samples is 3.7- and 5.7-fold longer, respectively, than to the central location of karst water samples. This analysis shows that the primary source of water inrush is karst water based on the discriminant criterion of the shortest distance and that a small part of the water inrush may be pore water. The training samples are also identified by FDA, and the discriminant accuracy is 100% in each category (Table 2), which illustrates that the discriminant functions are very effective and the discrimination results of the unknown samples are credible.

The groundwater interaction results in many hydrogeochemical effects with surrounding rock and groundwater from other aquifers, such as carbonate dissolution in the karst aquifer, chloride dissolution in the fissure aquifer, among others. These effects are the basis of the different hydrochemistry characteristics in different aquifers, even when there is a hydraulic connection to some extent between one aquifer and another. However, the hydrochemical characteristics in the local region of the same aquifer are roughly similar due to the same hydrogeochemical effects. The core concept of the FDA is the enlargement of the between-groups dispersion and

**Table 3** Distance between the location of water inrush point samples and the central location of other water samples

Samples of water inrush points	Distance to the central location of the pore water samples	Distance to the central location of the fissure water samples	Distance to the central location of the karst water samples
I1	4.34	7.09	2.24
I2	3.65	5.55	0.41
I4	4.32	6.32	0.68

the decrease of the within-groups dispersion in the training samples. These hydrochemistry characteristics are in agreement with the core concept of the FDA, which is the reason for the high identification accuracy.

*Mixing calculation*

According to the identification results of Piper diagram and FDA, there is no doubt that karst water is the major source of water inrush and that pore water may relate to water inrush. However, there is only a minuscule chance that fissure water relates to water inrush.

In this study we have assumed that water inrush is involved in karst water and pore water. The chloride ion does not react with other ions and is also not adsorbed in the void of rock mass and soil mass, so it is the most stable ion in the groundwater. Based on this premise, we establish the chloride mass balance equation (Eq. 12):

$$\begin{cases} Q_I c_I = Q_k c_k + Q_p c_p \\ Q_I = Q_k + Q_p \end{cases} \tag{12}$$

where  $Q_i$  is the rate of water inrush (m<sup>3</sup>/day);  $Q_k$  is the rate of karst water (m<sup>3</sup>/day);  $Q_p$  is the rate of pore water (m<sup>3</sup>/day),  $C_i$  is the concentration of the chloride ion of mine water in the water inrush point (mg/L);  $C_k$  is the concentration of the chloride ion in karst water (mg/L);  $C_p$  is the concentration of the chloride ion in pore water (mg/L).

According to Eq. 12, the mixing ratio of karst water to pore water ( $\lambda$ ) is obtained (Eq. 13).

$$\lambda = \frac{Q_k}{Q_p} = \frac{c_p - c_i}{c_i - c_k} \tag{13}$$

Because of the spatial variability of the chloride ion, the samples near the water inrush point are select to calculate the mixing ratio based on knowledge of the groundwater depression. These samples selected include P1, P4, P6, P7, K1, K3, K6, K7, and K9 (Table 2). The arithmetic mean value of each type of water sample is used in Eq. 13. The results show that mixing ratio of karst water to pore water is about 6.0, which directly indicates that karst water makes a large contribution to the rate of water inrush. The discrimination results of

groundwater dynamics and groundwater temperature also support this result. The results of the hydrogeochemistry discrimination not only indicate that the primary source of water inrush is karst water, but they also show that karst water accounts for 86% of the water inrush rates and pore water accounts for 14% of water inrush rates. This is the biggest advantage of this method compared with other methods.

Water samples taken from different locations of the same aquifer differ in their chemical constituents; even if water samples are taken at the same location, the chemical constituents of the samples differ at different times. Moreover, the water quantity from different areas of aquifers, including the pore aquifer and the karst aquifer, is not equivalent due to heterogeneity of the aquifer (Fig. 3). In addition, the anisotropy influences permeability of aquifers in different directions, which leads to the difference in flow rate in different directions in the process of water inrush. The anisotropy of karst aquifers is more remarkable than that of pore aquifers in general, as is the heterogeneity. Based on these factors, we note that the arithmetic mean value of chemical constituents certainly introduces some degree of error in the process of the mixing calculation. However, the error can be acceptable when combined with the identification results of groundwater dynamics and groundwater temperature.

Conventional hydrochemical analysis data are very easy to obtain in the mine due to the low test fee and the demand for hydrogeological exploration. Training samples do not meet special conditions in the application of FDA. Most importantly, the hydrochemistry discrimination not only has high identification accuracy, but also roughly evaluates the mixing ratio compared with other methods, such as the discrimination of groundwater dynamics, the discrimination of groundwater temperature, and others. This method has a potential for wide application due to its low cost and high efficiency compared with traditional methods.

## Conclusions

In the study reported here we apply three methods to determine the source of a water inrush. The results of these three methods consistently suggest that the primary source is karst water. The results of the hydrogeochemistry discrimination show that pore water is also involved in the water inrush and that the mixing ratio of karst water to pore water is about 6.0. Groundwater dynamics indicates that the recharge conditions of karst water is good and the static-reserves of karst water is abundant; The groundwater temperature suggests that karst water comes from the middle and lower part of karst aquifer. All three of these methods can discriminate the source of water inrush, each method has its own merits. However, based on merits, the hydrogeochemistry discrimination method is better than the other two.

Hydrogeochemistry discrimination by integrating the Piper diagram, FDA, and chloride mass balance have a powerful function for identifying water inrush sources and evaluating their contributions. The water inrush may involve water from a mixture of multiple sources due to fault activation and leakage recharge caused by variations in groundwater level and mining ground pressure. This method provides a relative satisfactory solution to this problem of determining water inrush, and it has more practical significance in engineering applications.

**Acknowledgements** This research is financially supported by the China National Natural Science Foundation (Grants 41272276, 41572222, 41602262 and 41430318), the China National Scientific and Technical Support Program (Grant 2016YFC0801800), the Beijing Natural Science Foundation (Grants 8162036 and 4142015), the Fundamental Research Funds for the Central Universities (Grant 2010YD02), the Innovation Research Team Program of the Ministry of Education (Grant IRT1085), the Project funded by China Postdoctoral Science Foundation (Grant 2016 M601172), and the State Key Laboratory of Coal Resources and Safe Mining. The authors would like to thank the editor and the reviewers for their constructive suggestions.

## References

- Abdula RA (2017) Geothermal gradients in Iraqi Kurdistan deduced from bottom hole temperatures. *Egypt J Pet* 26(3):601–608
- Chemseddine F, Dalila B, Fethi B (2015) Characterization of the main karst aquifers of the Tezben plateau, Tebessa region, northeast of Algeria, based on hydrogeochemical and isotopic data. *Environ Earth Sci* 74(1):1–10
- Chen HJ, Li XB, Liu AH (2009a) Studies of water source determination method of mine water inrush based on Bayes' multi-group stepwise discriminant analysis theory. *Rock Soil Mech* 30(12):3655–3659 (in Chinese)
- Chen HJ, Li XB, Liu AH et al (2009b) Identifying of mine water inrush sources by fisher discriminant analysis method. *J Cent South Univ* 40(4):1114–1120 (in Chinese)
- Chen LW, Gui HR, Yin XX et al (2010) The standard type trace elements and the discriminant model of water bursting source in the Linhuan coal district. *Hydrogeol Eng Geol* 37(3):17–22 (in Chinese)
- Chen LW, Feng XQ, Xie WP et al (2016) Prediction of water-inrush risk areas in process of mining under the unconsolidated and confined aquifer: a case study from the Qidong coal mine in China. *Environ Earth Sci* 75(8):1–17
- Chen YM, Chen ZH, Yu KB (2013) To identify the recharge conditions of karst groundwater in mining area by means of groundwater table and water temperature data: a case in Makeng iron mine. *Fujian Carsologica Sinica* 32(1):64–72 (in Chinese)
- Cheng QS (1997) Attribute recognition theoretical model with application. *Acta Sci Nat Univ Pekin* 33(1):12–20 (in Chinese)
- Chiang LH, Kotanchek ME, Kordon AK (2004) Fault diagnosis based on fisher discriminant analysis and support vector machines. *Comput Chem Eng* 28(8):1389–1401
- Feng LJ, Li JS, Shao GQ (2002) The application of Adaline in recognition of mine water quality types. *Coal Geol Exploration* 30(4):35–37 (in Chinese)
- Gu HY, Ma FS, Guo J et al (2017) Assessment of water sources and mixing of groundwater in a coastal mine: the Sanshandao gold mine, China. *Mine Water Environ*. <https://doi.org/10.1007/s10230-017-0458-0>

- Gültekin F, Ersoy AF, Hatipoglu E et al (2013) Quality assessment of surface and groundwater in Solaklı basin (Trabzon, Turkey). *Bull Eng Geol Environ* 72(2):213–224
- Guo H, Nandi AK (2006) Breast cancer diagnosis using genetic programming generated feature. *Pattern Recogn* 39(5):980–987
- Huang PH, Chen JS (2011) Fisher identify and mixing model based on multivariate statistical analysis of mine water inrush sources. *J China Coal Soc* 36(S1):131–136 (in Chinese)
- Kuroda K, Hayashi T, Do TD et al (2017) Groundwater recharge in suburban areas of Hanoi, Vietnam: effect of decreasing surface-water bodies and land-use change. *Hydrogeol J* 25(3):727–742
- Li LP, Lei T, Li SC et al (2014) Risk assessment of water inrush in karst tunnels and software development. *Arab J Geosci* 8(4):1843–1854
- Li Y, Hu FS, Xue ZQ et al (2015) Hydrogeochemical and isotopic characteristics of groundwater in the salt chemical industrial base of Guyuan City, northwestern China. *Arab J Geosci* 8(6):3427–3440
- Li J, Li FD, Liu Q (2017) PAHs behavior in surface water and groundwater of the Yellow River estuary: evidence from isotopes and hydrochemistry. *Chemosphere* 178:143–153
- Lin Y, Wu YZ, Pan GY et al (2015) Determining and plugging the groundwater recharge channel with comprehensive approach in Siwan coal mine. *North China coal basin. Arab J Geosci* 8(9):1–12
- Liu J, Liu D (2012) Source identification of water inrush in tunnel based on SVM. *Hydrogeol Eng Geol* 34(1):33–38 (in Chinese)
- Liu QS, Huang R, Lu HQ et al (2003) Kernel-based nonlinear discriminant analysis for face recognition. *J Comput Sci Technol* 18(6):788–795
- Liu YP, Yamanaka T (2012) Tracing groundwater recharge sources in a mountain–plain transitional area using stable isotopes and hydrochemistry. *J Hydrol* 464–465(10):116–126
- Ma D, Miao XX, Bai HB et al (2016) Effect of mining on shear sidewall groundwater inrush hazard caused by seepage instability of the penetrated karst collapse pillar. *Nat Hazards* 82(1):73–93
- Ma L, Qian JZ, Zhao WD (2014) An approach for quickly identifying water-inrush source of mine based on GIS and groundwater chemistry and temperature. *Coal Geol Exploration* 42(2):49–53 (in Chinese)
- Mathurin FA, Åström ME, Laaksoharju M et al (2012) Effect of tunnel excavation on source and mixing of groundwater in a coastal granitoidic fracture network. *Environ Sci Technol* 46(23):12779–12786
- Meng ZP, Li GQ, Xie XT (2012) A geological assessment method of floor water inrush risk and its application. *Eng Geol* 143:51–60
- Najib S, Fadili A, Mehdi K et al (2017) Contribution of hydrochemical and geoelectrical approaches to investigate salinization process and seawater intrusion in the coastal aquifers of Chaouia, Morocco. *J Contam Hydrol* 198:24–36
- Négre P, Petelet-Giraud E, Barbier J et al (2003) Surface water–groundwater interactions in an alluvial plain: chemical and isotopic systematics. *J Hydrol* 277(3):248–267
- Petitta M, Primavera P, Tuccimei P et al (2011) Interaction between deep and shallow groundwater systems in areas affected by Quaternary tectonics (Central Italy): a geochemical and isotope approach. *Environ Earth Sci* 63(1):11–30
- Potot C, Féraud G, Schärer U et al (2012) Groundwater and river baseline quality using major, trace elements, organic carbon and Sr–Pb–O isotopes in a Mediterranean catchment: the case of the lower Var Valley (south-eastern France). *J Hydrol* 472:126–147
- Qian JZ, Wang L, Ma L et al (2016) Multivariate statistical analysis of water chemistry in evaluating groundwater geochemical evolution and aquifer connectivity near a large coal mine, Anhui, China. *Environ Earth Sci* 75(9):1–10
- Redwan M, Adbel Moneim AA (2015) Factors controlling groundwater hydrogeochemistry in the area west of Tahta, Sohag, upper Egypt. *J Afr Earth Sci* 118:328–338
- Subyani AM (2004) Use of chloride-mass balance and environmental isotopes for evaluation of groundwater recharge in the alluvial aquifer, Wadi Tharad, western Saudi Arabia. *Environ Geol* 46(6–7):741–749
- Sui WH, Liu JY, Yang SG et al (2011) Hydrogeological analysis and salvage of a deep coalmine after a groundwater inrush. *Environ Earth Sci* 62(4):735–749
- Sun LH (2013) Statistical analysis of hydrochemistry of groundwater and its implications for water source identification: a case study. *Arab J Geosci* 7(9):3417–3425
- Sun WJ, Zhou WF, Jiao J (2016) Hydrogeological classification and water inrush accidents in china's coal mines. *Mine Water Environ* 35(2):214–220
- Wang LF, Hu FS, Yin LH et al (2013) Hydrochemical and isotopic study of groundwater in the Yinchuan plain, China. *Environ Earth Sci* 69(6):2037–2057
- Wang TT, Jeng FS, Wei L (2011) Mitigating large water ingresses into the new Yungchuen tunnel. Taiwan. *Bull Eng Geol Environ* 70(2):173–186
- Wang XY, Ji HY, Wang Q et al (2016) Divisions based on groundwater chemical characteristics and discrimination of water inrush sources in the Pingdingshan coalfield. *Environ Earth Sci* 75(10):1–11
- Wu J, Li SC, Xu ZH et al (2016) Flow characteristics and escape-route optimization after water inrush in a backward-excavated karst tunnel. *Int J Geomech* 17(4):04016096
- Wu Q, Wang MY (2006) Characterization of water bursting and discharge into underground mines with multilayered groundwater flow systems in the North China coal basin. *Hydrogeol J* 14(6):882–893
- Wu Q, Zhao DK, Wang Y et al (2017) Method for assessing coal-floor water-inrush risk based on the variable-weight model and unascertained measure theory. *Hydrogeol J*. <https://doi.org/10.1007/s10040-017-1614-0>
- Xu JM, Shao JL (1988) Lecture on groundwater management: the second lesson: the classification of groundwater system and the function of unit impulse response. *Geotech Investig Survey* (2):46–52 (in Chinese)
- Xu B, Zhang Y, Jiang L (2012) Coupled model based on grey relational analysis and stepwise discriminant analysis for water source identification of mine water inrush. *Rock Soil Mech* 33(10):3122–3128 (in Chinese)
- Yang YG, Huang FC (2007) Water source determination of mine inflow based on non-linear method. *J China Univ Min Technol* 36(3):283–286
- Yang YY, Xu YS, Shen SL et al (2015) Mining-induced geo-hazards with environmental protection measures in Yunnan, China: an overview. *Bull Eng Geol Environ* 74(1):141–150
- Yin SX, Zhang JC, Liu DM (2015) A study of mine water inrushes by measurements of in situ stress and rock failures. *Nat Hazards* 79(3):1961–1979
- Zeng YF, Liu SQ, Zhang W et al (2016a) Application of artificial neural network technology to predicting small faults and folds in coal seams, China. *Sustain Water Resour Manag* 2(2):175–181
- Zeng YF, Wu Q, Liu SQ et al (2016b) Vulnerability assessment of water bursting from Ordovician limestone into coal mines of China. *Environ Earth Sci* 75(22):1431. <https://doi.org/10.1007/s12665-016-6239-4>
- Zhang JC (2005) Investigations of water inrushes from aquifers under coal seams. *Int J Rock Mech Min Sci* 42(3):350–360
- Zhang RG, Qian JZ, Ma L et al (2009) Application of extension identification method in mine water bursting source discrimination. *J China Coal Soc* 34(1):33–38 (in Chinese)
- Zhang Y, Ma YD, Wu H (2014) EW-UCA model for identifying mine's water-filled source and its application. *Hydrogeol Eng Geol* 41(4):32–37 (in Chinese)
- Zhou J, Shi XZ, Wang HY (2010) Water-bursting source determination of mine based on distance discriminant analysis model. *J China Coal Soc* 35(2):278–282 (in Chinese)
- Zhou J, Li XB, Shi XZ et al (2011) Predicting pillar stability for underground mine using fisher discriminant analysis and SVM methods. *Trans Nonferrous Metals Soc China* 21(12):2734–2743
- Zhou ZQ, Li SC, Li LP et al (2015) An optimal classification method for risk assessment of water inrush in karst tunnels based on grey system theory. *Geomech Eng* 8(5):631–647